Materials Today Bio 28 (2024) 101243

Contents lists available at ScienceDirect

Materials Today Bio

journal homepage: www.journals.elsevier.com/materials-today-bio

Homologous cell membrane-based hydrogel creates spatiotemporal niches to improve outcomes of dysregulated chronic wound healing

Yijuan Ding [1], Qi Jia [1], Ziwen Su, Heying Chen, Jialing Ye, Dafeng Xie, Yubo Wu, Haiyan He, Yanlin Peng, Yilu Ni [*]

The M.O.E. Key Laboratory of Laboratory Medical Diagnostics, The College of Laboratory Medicine, Chongqing Medical University, #1 Yixueyuan Road, Yuzhong District, Chongqing, 400016, China

1. Introduction

Inflammation, a process that establishes an immune barrier against invasion by foreign microorganisms, is important in wound healing. The primary purpose of early inflammation is to remove extraneous particles, invasive microbes, and damaged cells and tissues [1–3]. However, excessive inflammation can lead to various pathogenic disturbances in the microenvironment of chronic wounds and even severe symptoms that might cause major problems to the patient [4,5]. In the inflammatory phase, macrophages are phagocytic cells in charge of clearing bacteria and damaged cell debris, especially their phenotype evolves with the progression of inflammation [6]. During this process, they are phenotypically classified as pro-inflammatory macrophages, or referred to as "M1" macrophages, having significant impact on the preliminary wound sanitization. Beyond that, a timely transition of macrophage population to anti-inflammatory phenotype (referred to as "M2" macrophages) is also necessary, as the ending of inflammation initiates subsequent proliferative phase and benefits the overall healing process [7]. However, insufficient bacteria clearance or morbid dysfunction in chronic wounds are often inducing macrophages to dampen the immune system and ameliorate the inflammation as if they believe the inflammation is not controlled effectively. Thus, modulating the phenotypic differentiation of macrophages to avoid over-inflammation can prevent collateral cell death and shorten or significantly improve the healing process [8].

Until now, various methods have been developed to induce the differentiation of macrophages into specific subtypes, such as extracellular vesicles, hydrogel scaffolds, and biofunctionalized nanoparticles [9–12]. Recently, the utilization of cell membrane-based therapeutics has emerged with great potential for specific and effective modulation over target cells, including dendritic cells (DCs), lymphocyte, and even cancer cells [13–18]. Likewise, macrophages can be easily manipulated by cell membranes [19]. Their switching character in phenotype makes them vulnerable to homologous cell membranes derived from parent macrophages in different subsets, either to enhance their functions by the same phenotypic membranes, or to be totally reversed by the membranes with "opposite" phenotype [20]. Although the molecular mechanism is inexplicit and still in the early phases, current research has elucidated that intrinsic modulatory effect in macrophage membranes is mostly dependent on the displaying of membranous molecules, which can induce increased expression of inherent molecules in the membrane-treated macrophages and regulate their activities [21]. Based on this, we previously reported that macrophage membranes can circumvent limitations in traditional biomaterials such as low bioactivity and simple biofunctions for skin wound treatment [22]. To take further advantage of the on-call switching effect inserted by macrophage membranes, a more delicate administration should be made to achieve an on-demand regulation on the phenotype of macrophages depending on the changing phase of *in vivo* microenvironment.

Here, we fabricate a hydrogel dressing loaded with homologous cell membranes derived from M2 macrophages and transforming growth factor-β (TGF-β), to implement precise and controllable modulation over the inflammatory phase for addressing unmet medical needs in chronic wound healing (Scheme 1). The hydrogel is prepared from methacrylated hyaluronic acid (HAMA), it provides well-maintenance for the membrane and growth factor cargos to inflict their stimulation on localized target cells. It also coats a screening barrier on the uncovered wounds against any further bacterial infection, offering an efficient wound clearance for first arrived neutrophils. Moreover, the HA-based hydrogel can enhance the expression of pro-inflammatory factors produced by M1 macrophages [23]. Importantly, the hydrogel is internally embellished with M2 macrophage membranes collected from homologous bone marrow-derived macrophages (BMDMs). Together, they create spatiotemporal niches that repolarize pro-inflammatory M1

* Corresponding author. Chongqing Medical University, #1 Yixueyuan Road, Yuzhong District, Chongqing, 400016, China.
E-mail address: nyl@cqmu.edu.cn (Y. Ni).
[1] These authors contributed equally to this work.

https://doi.org/10.1016/j.mtbio.2024.101243
Received 20 June 2024; Received in revised form 25 August 2024; Accepted 12 September 2024
Available online 14 September 2024

macrophages into anti-inflammatory M2 phenotype in an epigenetic manner. Meanwhile, TGF-β is additionally released to promote the proliferation of fibroblasts, offering a timely transition from inflammation to the subsequent proliferative phase. Our work provides a safe and effective strategy to focus on the improvement of inflammation in a time sequential mode. This method is supported by profound theoretical basis, and has a great prospect for clinical applications in chronic wound healing therapeutics.

2. Materials and methods

2.1. Materials

Dulbecco's modified Eagle's medium (DMEM) was purchased from Gibco (USA). Fetal bovine serum (FBS) was obtained from Bio-channel (China). Phenylmethyl-sulfonyl fluoride (PMSF), penicillin-streptomycin solution, Calcin-AM/PI cell activity staining dye, and cytotoxicity detection kits were purchased from Beyotime (China). Trypsin was purchased from Thermo (USA). Hyaluronic acid (HA, 20–40 kDa) was obtained from BLOOMAGE BIOTECH (China). Type I collagenase, methacrylic anhydride (MA), and lipopolysaccharide (LPS) were provided by Sigma Aldrich (USA). Mouse recombinant granulocyte macrophage colony-stimulating factor (GM-CSF) was provided by Peprotech (USA). Interleukin-4 (IL-4) and interferon-γ (IFN-γ) were purchased from Nearshore Protein (China). Cell counting kit (CCK8) was purchased from MedChemexpress (USA). The polyvinylidene fluoride (PVDF) membrane was purchased from Millipore (USA). Anti-CD45-APC-Cy7, anti-CD11b-FITC, and anti-CD86-PE were purchased from BD Biosciences (USA). Anti-CD206-Alexa 647 was purchased from Biolegend (USA). Anti-tublin was obtained from TransGen Biotech (China). Anti-iNOS was purchased from Abcam (UK). Anti-ARG1 was purchased from Santa Cruz Biotechnology (USA). HRP-conjugated Affinipure Goat Anti-Rabbit IgG (H + L), HRP-conjugated Affinipure Goat Anti-Mouse IgG (H + L) were purchased from Proteintech Group (USA). *Escherichia coli* (*E. coli*) and *Staphylococcus aureus* (*S. aureus*) were kindly provided by Prof. Deqiang Wang, College of Laboratory Medicine, Chongqing Medical University.

2.2. Mice and cell lines

BALB/c mice (female, 5–7 weeks) were purchased from Chongqing Medical University (Chongqing, China). The animal study has been

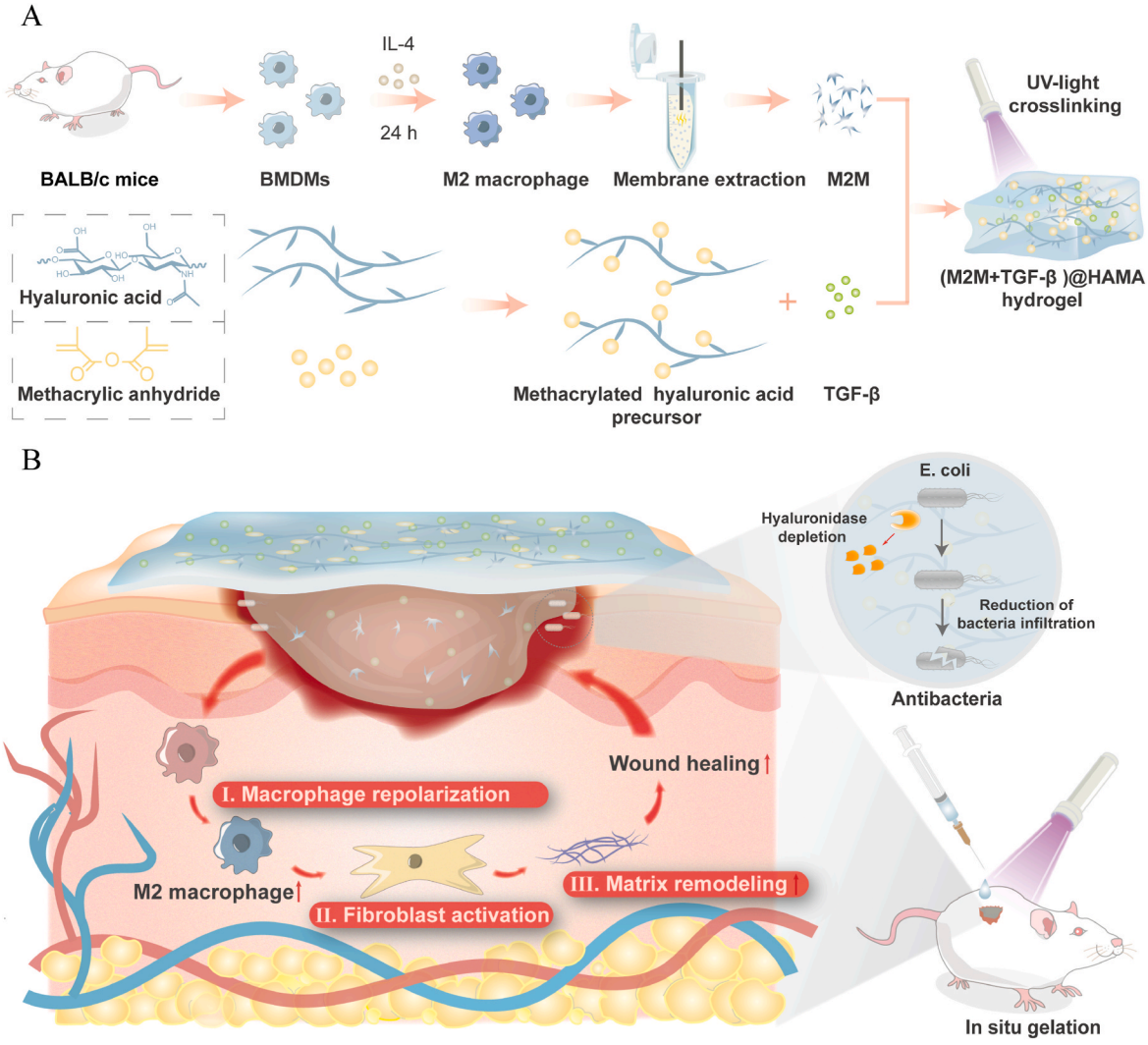

Scheme 1. Schematic illustration of (M2M + TGF-β)@HAMA hydrogel dressing that promotes dysregulated chronic wound healing. A) Derivation of cell membrane from M2 macrophage, preparation of methacrylated hyaluronic acid hydrogel, and synthesis of (M2M + TGF-β)@HAMA hydrogel dressing. B) Mechanical cues of (M2M + TGF-β)@HAMA hydrogel dressing in wound healing process. The hydrogel protects the open wound from repeated bacterial infections, reprograms endogenous monocytes and M1 macrophages into an M2-phenotype, and enhances fibroblastic proliferation and migration to improve outcomes of dysregulated chronic wound healing.

reviewed and approved by the Institutional Animal Care and Use Committee (IACUC) of the School of Medicine of Chongqing Medical University. RAW 264.7 macrophages were cultured in DMEM medium containing 10 % fetal bovine serum and 1 % penicillin-streptomycin (10000 U/mL).

2.3. Derivation of bone marrow-derived macrophages (BMDMs)

Female BALB/c mice were killed and soaked in 75 % alcohol for 5 min. The back skin from the hind legs was harvested and muscle attachments were removed, the intact femurs and tibia were also collected. Complete bones were soaked in PBS containing 10 % penicillin-streptomycin for 5 min and then washed with PBS for 3 times. The joints at both ends were cut off, and the bone marrow cavity was exposed. Using a 1 mL syringe to completely flush the bone marrow cavity with DMEM until the cavity turned white. After centrifugation at 400*g* for 5 min, red blood cells (RBCs) were lysed with lysis buffer. The rest of cells were collected and cultured in a 100 mm culture dish with DMEM containing 20 % fetal bovine serum and 1 % penicillin-streptomycin. After 24 h, the cells were further cultured with conditioned medium (DMEM containing 20 % fetal bovine serum, 1 % penicillin-streptomycin, and 20 ng/mL of GM-CSF) for 7 days. After 1 week of conditioned culture, the cells were collected as BMDMs for further use. M1 macrophages can be further obtained from IFN-γ (20 ng/mL) and LPS (20 ng/mL) treatment, and M2 macrophages can be obtained from IL-4 (20 ng/mL) treatment.

2.4. Cell membrane preparation

The M2-type macrophages were first collected and washed with PBS for 3 times. After centrifugation at 400*g* for 5 min, the cells were re-suspended in a hypotonic solution containing 10 mM PMSF. The cell suspension was incubated on ice for 10 min, followed by ultrasonic processing on ice bath for 6 min. And then the solution was centrifuged at 700 g for another 10 min. The supernatant was collected and centrifugated at 14, 000 g for 40 min. The precipitate was collected and freeze-dried as the cell membranes derived from M2 macrophages, and stored at −80 °C for further use. The protein concentration of cell membrane was determined by bicinchoninic acid assay (BCA), and the membrane concentration was controlled at 100 μg/mL in all the *in vitro* and *in vivo* experiments, unless otherwise specified.

2.5. Hydrogel preparation and characterization

The HA powder (0.5 g) was added in 50 mL distilled water and stirred continuously until completely dissolved. MA (2.4 mL) was added dropwise to the solution, and the pH value was controlled at 8–10 using 5 M sodium hydroxide solution, the mixture reacted for 24 h at 4 °C. After the reaction was completed, the mixture was dialyzed against deionized water in a dialysis bag with the MWCO of 12–14 kDa at 4 °C for 3 days, and was then freeze-dried at −50 °C for another 3 days. The freeze-dried product was HAMA power, and 10 mg HAMA was dissolved in 1 mL PBS to obtain 10 mg/mL of HAMA solution for further use.

For ^{1}H nuclear magnetic resonance (^{1}H NMR) analysis, the freeze-dried HAMA (5 mg) was dissolved in D_2O (500 μL). Then the sample was analyzed using 400 MHz nuclear magnetic resonance spectrometer (Bruker, Germany). For swelling ratio assay, the HAMA hydrogels were freeze-dried and soaked in 1 mL PBS. At specific time points, the hydrogels were taken out and removed from surface moisture with a filter paper. The weight of each hydrogel was measured, and the swelling ratio was calculated as: Swelling ratio = $(W_2 - W_1)/W_1 \times 100$ %, where W_2 is the real-time weight of hydrogel sample, and W_1 is the initial weight of hydrogel sample. For deswelling ratio assay, the dry weight (M_0) of freeze-dried hydrogels were first weighed at 0 h. And then the hydrogels were swollen to constant weight (M_k) and placed in an environment of 37 °C and 50 % humidity. The hydrogels were weighed every 12 h (as M_t), and the water retention rate was calculated as: Water retention rate = $(M_t - M_0)/(M_k - M_0) \times 100$ %. For morphology observation, the hydrogel samples were immersed in deionized water to swelling equilibrium, frozen in liquid nitrogen for 15 min, and freeze-dried at −50 °C for 24 h. The cross section of the dry sample was sputtered with gold and observed using a scanning electron microscopy (SEM, Sigma 300, Zeiss, Germany).

2.6. Bacteria culture

The Gram-negative bacteria of *E. coli* and Gram-positive *S. aureus* were used. Single colonies grown on Luria-Bertani (LB) plates were inoculated into the 5 mL sterile MuellerHinton broth (MHB), shaken at 200 rpm and 37 °C for 12 h. An ultraviolet–visible spectrophotometer was used to calculate the bacterial count by measuring the absorbance at 600 nm. Dilute the bacterial solution 1×10^5 times to obtain bacterial suspension, and then mix 100 μL of the bacterial suspension with 900 μL PBS, and 900 μL HAMA precursor solution of 5, 10, 15, and 20 mg/mL, respectively. All the mixtures were incubated at 37 °C for 4 h, and the mixing solution (100 μL) was added onto the LB agar, the bacterial growth on the plate was photographed 24 h later.

2.7. CCK8 assay

The cells were seeded in the 96-well plate at 5×10^3 cells/well density. After 4 h of incubation, the cells were treated with HAMA and M2M, respectively. At the time intervals of 0, 12, 24, and 48 h, the medium was discarded. And the cells were collected and washed with PBS, followed by staining with freshly prepared CCK8 solutions at 37 °C for 2 h. The absorbance used to calculate cell viability was 450 nm.

2.8. Living/dead cell staining

The BMDMs and RAW264.7 cells were inoculated in a confocal dish at a density of 2×10^5 cells/well. After 4 h, the cells were incubated with HAMA and M2M, respectively. After another 48 h, the medium was discarded, and the cells were washed with PBS for 3 times. The freshly prepared Calcin-AM/PI dyeing solution was used to stain the cells at 37 °C for 15 min. The living/dead cells were observed by confocal laser scanning microscopy (CLSM, Leica, TCSAP8Dmi8).

2.9. Hemolysis test

The whole blood (2 mL) of BALB/c mice was drawn and added into the heparin sodium anticoagulant centrifuge tube, mixed with the same amount of normal saline, and centrifuged at 3, 000 rpm for 15 min. The precipitation was washed 3 times with the same volume of normal saline to obtain red cell suspension (RCS). The diluent of 4.0 % RCS was prepared by mixing RCS (1 mL) with normal saline (24 mL) and stored at 4 °C for further use. Add 1 mL RCS diluent with HAMA, M2M, M2M@HAMA, and (M2M + TGF-β)@HAMA into the centrifuge tube, respectively, or add 1 mL RCS diluent with HAMA hydrogel (20 μL) in concentration gradient of 5, 10, 15, and 20 mg/mL into the centrifuge tube, respectively. The normal saline was set as the negative control group, and ultra-pure water was set as the positive control group. After incubation at 37 °C for 1 h, the solution was centrifuged at 3, 000 rpm for 15 min, and the optical density value (OD value) of supernatant was determined at 540 nm. The hemolysis rate (H_r) was calculated as: $H_r = (OD_E - OD_N)/(OD_P - OD_N) \times 100$ %, where OD_E was the absorbance of analytes, OD_N was the absorbance of negative control, and OD_P was the absorbance of positive control.

2.10. Hyaluronidase depleting analysis

The HAMA hydrogels (300 μL, 10 mg/mL) weighed as M_0 were added into 1 mL hyaluronidase solutions of 1, 000 U/mL, 100 U/mL, 10

U/mL, 1 U/mL, and 1 mL bacterial suspension of 1×10^6 CFU/mL, respectively. The mass of hydrogels was then continuously weighed every 24 h as M_t. The hyaluronidase depleting rate was in consistency with the weight loss of HAMA hydrogels. Weight loss = $(M_0 - M_t)/M_0 \times 100$ %.

2.11. Western blot

The cells were seeded in 6-well plates at 2×10^5 cells/well density, and treated by M2M for 24 h. And then the cells were washed with PBS for 3 times, the protein was extracted from the sample with 1 % SDS cracking buffer, and its concentration was determined by using a BCA protein quantitative kit. The total protein concentration was 10–20 μg for electrophoresis. The volume of the protein and the corresponding volume of the 5 × SDS loading buffer were calculated from the determined concentration. After mixing, the sample was heated in a metal bath at 95 °C for 10 min. The sodium dodecyl sulphate-polyacrylamide gel was prepared in advance, and target protein was isolated at constant pressure of 80 V after being added to the protein sample. Subsequently, the protein was transferred to the PVDF membrane at a constant current of 300 mA. The membrane was closed with 5 % bovine serum albumin at room temperature for 1 h, and then incubated with primary antibodies anti-tublin (1: 4000), anti-ARG1 (1: 1000), or anti-iNOS (1: 1000), overnight at 4 °C. The next day, the TBST washing film was used for 5 times (5 min each time), and was then combined with the secondary antibody at room temperature for 1.5 h. The images were taken by a Smart-ECL system with chemiluminescence imager.

2.12. Animal study

The animal model of skin wound repair was established in female BALB/c mice. The mice were randomly divided into 5 groups named as Ctr, HAMA, M2M, M2M@HAMA, and (M2M + TGF-β) @HAMA. The concentration of TGF-β was controlled at 8 ng/mL. The skin wounds with a diameter of 8 ± 0.5 mm were punched using a perforating tool on both sides of the back skin.

2.13. Flow cytometry analysis

The wounded skin was collected at 1 and 2 d. The retrieved samples were incubated in collagenase I (2.5 mg/mL) solution at 37 °C for 60 min, and was continuously stirred. And then the solution was filtered through a 70 μm aperture filter. The obtained single-cell suspension was washed 3 times with PBS and then incubated with anti-CD45-APC-Cy7, anti-CD11b-FITC, anti-CD86-PE, and anti-CD206-Alexa647 at 4 °C for 30 min. The single cell suspension was analyzed by flow cytometry.

2.14. Statistical analysis

All data were expressed as mean ± standard deviations (SD). Student's t-test was used to statistically analyze the data obtained from the experiments. '*' is the intergroup comparison. Significant differences are indicated as *, $p < 0.05$; **, $p < 0.01$; ***, $p < 0.001$. At least 3 parallel samples were set for each group of experimental test samples.

3. Results and discussion

3.1. Hydrogel preparation and characterization

The stimuli-responsive wound dressing can increase therapeutic efficacy significantly while simultaneously reducing adverse side effects by enabling the activation of function locally at the sites of interest [24]. Hyaluronic acid (HA) has rapidly grown as a major component and serves as a versatile building block for stimuli-responsive wound dressing, due to its highly modifiable structure of repeated disaccharide units of β-D-glucuronic acid and n-acetyl-d-glucosamine, linked alternately by β-1, 3 and β-1, 4 glucoside bonds [25]. In this work, hyaluronic acid is first methacrylated as HAMA according to previous study (Fig. 1A) [26]. ^{1}H NMR results in Fig. 1B confirm the successful modification of HA, as the specific signaling peaks at 5.5–6.5 ppm referring to ester bond of methacrylic anhydride are shown in HAMA. And then, HAMA precursor can be crosslinked in the presence of a photopolymerization initiator (Fig. S1). As shown in Fig. 1C, the swelling ratio of HAMA hydrogel in physiological microenvironment (PBS) decreases with the increment of solid content, and reaches swelling equilibrium within 10 h. Meanwhile, water retention increases as the solid content increases according to deswelling results (Fig. 1D). In SEM images (Fig. 1E), the hydrogels are shown in classic polymeric morphology, with porous and leaf-like structure, the pore size increases with the decrease of solid content. And lower solid content also leads to lower viscosity (Fig. S2). However, when the concentration reaches lower than 5 mg/mL, the shape of hydrogel can hardly be well-maintained (Fig. 1F). In addition, the lower concentration also leads to poorer antibacterial effect against *E. coli* (Fig. 1G and H) and *S. aureus* (Fig. S3). This solid content-dependent anti-infection could be possibly due to the easy degradation of HA with low molecular weight causing over-depletion of bacteria-produced hyaluronidase, reducing bacterial infiltration [27]. Thus, the weighing method is utilized to determine the hyaluronidase depleting ability of HAMA, verifying the equivalent hyaluronidase secretion of *E. coli* with 1 U/mL of hyaluronidase standard solution, as well as the over-depleting phenomenon in HAMA-treated *E. coli* (Fig. 1I). Consequently, the hydrogel of 10 mg/mL is selected based on the above data for further study, owing to its appropriate physical properties, antibacterial effect, and loading capacity (Fig. 1). The cell membranes derived from M2 macrophages are then loaded in the hydrogel, named as M2M@HAMA. The SEM images in Fig. 1J demonstrate a dispersed and uniformly arranged distribution of cell membranes. Generally, HAMA is proven a reliable and cogent building block to provide supporting scaffold for the wound dressing with superior gelation properties, delivering capacity, and a favorable anti-infection effect.

3.2. Cell membranes derived from M2 macrophages regulate polarization of macrophages in different subtypes

In the inflammatory site of wounds, disparate environmental cues are reconciled with one another to dampen or drive inflammatory transformation [28]. Monocyte-derived macrophages are driven into pro-inflammatory M1 state, which associate with the periphery niche and elicit marked inflammatory changes in nearby cells [29]. A two-way dialogue of communication between macrophages and their environment can rewire downstream events non-genetically and skew the morphogenetic course of the wounded tissue [30]. Previous, cell membranes are proven an effective candidate for creating an epigenetic microenvironment that reverses the well-established inflammatory niche, as well as the polarizing status of macrophages [22]. In this work, a spatiotemporal platform offered by hydrogel dressing is built to trigger the cell membrane-mediated epigenetic changes in endogenous macrophages that help restoring the dysregulated wound healing. First, BMDMs ($CD11b^+$) are successfully obtained from BALB/c mice and polarized into M2-type ($CD206^+$) in conditioned medium, that $CD11b^+$ cells account for 84.04 % and $CD206^+$ cells account for 92.05 % of the cell population (Fig. 2A). In the BMDMs-induced M2 macrophages, the WB assay further confirms their phenotypes by showing a high expression of ARG1 (M2 marker) and a low expression of iNOS (M1 marker) in Fig. 2B. Subsequently, these M2-type macrophages are then lysed by hypoosmotic and ultrasonic crushing, and their cell membranes (M2M, displayed in Fig. 2C) are isolated as epigenetic drivers in the context of their potential to exert repolarizing effect. As expected, the cell membranes show a good inheritance of protein profile from the parent M2 macrophages, with no hetero proteins found (Fig. 2D). In addition to support the theory that M2 membranes can induce an M2 polarization,

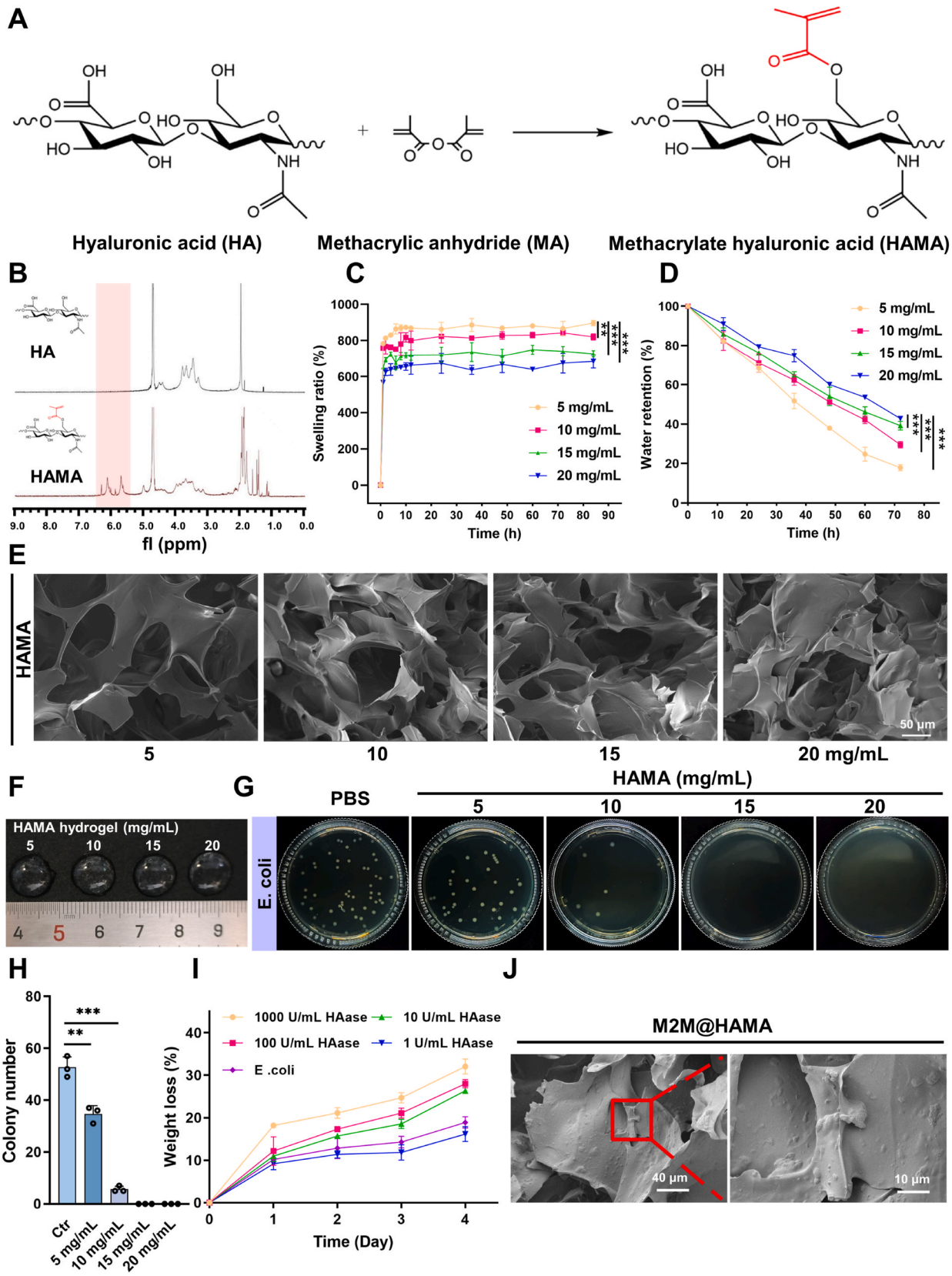

Fig. 1. Preparation and characterization of HAMA and M2M@HAMA hydrogel. A) The methacrylation formula of HA. B) ^{1}H NMR spectrum of HA and HAMA. C) Swelling ratio curve and D) deswelling ratio curve of HAMA hydrogel. E) SEM images of HAMA hydrogels. Scale bar = 50 μm. F) Photographs of HAMA hydrogel. G) Antibacterial effect and H) the corresponding quantitative data of HAMA hydrogel on *E. coli*. I) The hyaluronidase depleting ability of HAMA hydrogel. J) SEM images of M2M@HAMA hydrogel. Scale bar = 40 or 10 μm. Data are presented as mean ± SD (n = 3). 'Ctr' represents untreated group. '*' is the intergroup comparison. *, $p < 0.05$; **, $p < 0.01$; ***, $p < 0.001$.

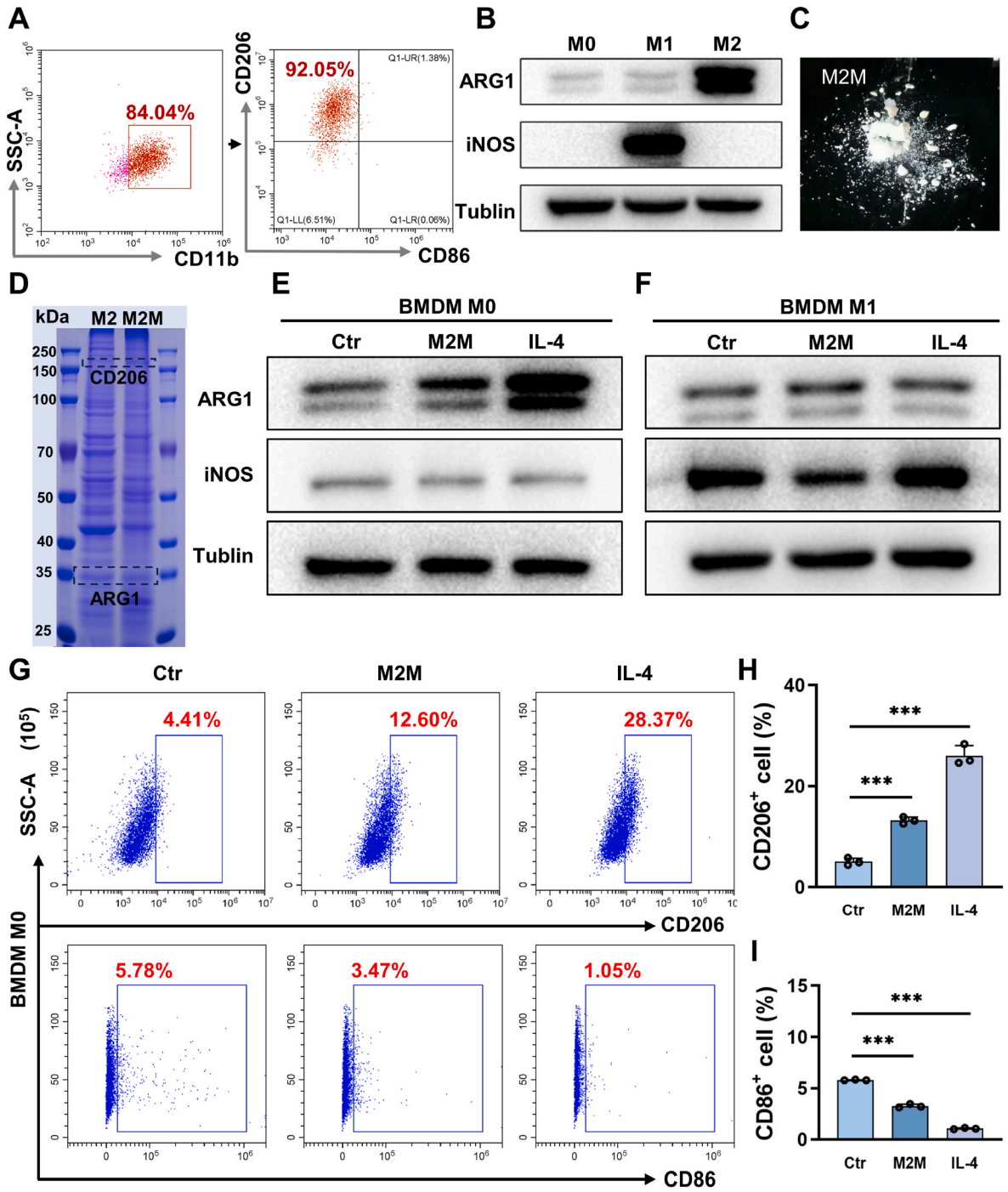

Fig. 2. Preparation and characterization of cell membranes derived from M2 macrophages (BMDMs). A) Flow cytometry analysis of M2 macrophages derived from BMDMs. B) The ARG1 and iNOS expression of BMDMs in M0, M1, and M2 phenotype. C) The photograph of cell membranes derived from M2 macrophages. D) The SDS-PAGE electrophoresis pattern of M2M and M2 macrophages. E), F) The ARG1 and iNOS expression of BMDMs in M0 and M1 phenotype after different treatments for 24 h. G) Flow cytometry analysis of M0 macrophages after different treatments for 24 h and the corresponding quantification of H) $CD206^+$ and I) $CD86^+$ cells. Data are presented as mean ± SD (n = 3). 'Ctr' represents untreated group. '*' is the intergroup comparison. *, $p < 0.05$; **, $p < 0.01$; ***, $p < 0.001$.

BMDMs are treated with M2M *in vitro* for 24 h. As shown in Fig. 2E and F, both naive M0 macrophage and pro-inflammatory M1 macrophage are repolarized into anti-inflammatory M2 phenotype after M2M treatment, marked by the upregulation of ARG1 expression and the downregulation of iNOS expression. It is noteworthy that our results show an evident polarization of M0 macrophage into active M2 state, but the M1-M2 transition is not that obvious. That is to say, the relatively more mature M1-type macrophages are more difficult to be reversed in cellular phenotype. In fact, it has been reported that M1 macrophages could not be repolarized into M2-type by IL-4, the most effective cytokine for laboratory use that activates M2 polarization [31], which is reconciled with our data in Fig. 2F. Somehow, M2M shows a degree of reprogramming M1 macrophages, that the minor upregulation of ARG1 and downregulation of iNOS expression can still be seen. The same conclusions are supported by flow cytometry results in Fig. 2G–I and Fig. S4, that upregulation of CD86 and downregulation of CD206 are both found in M2M – and IL-4-treated M0 macrophages to confirm the M0-M2 polarization, but such results are only seen in M2M-treated M1

macrophages. For more solid evidence, identical WB experiments are performed in laboratory RAW 264.7 macrophages, and similar results are demonstrated in Figs. S5 and S6. These results not only confirm that cell membranes derived from M2 macrophages can reprogram different subtypes of allogeneic macrophages, but also suggest to a non-genetic modification over the context-dependent macrophages via an epigenetic manner.

3.3. The hydrogel dressing shows excellent biocompatibility

As a natural polymer, HA belongs to a group of heteropolysaccharides called glycosaminoglycans (GAGs), which can be found in human vitreous body, joints, umbilical cord, skin, and connective tissue etc [32]. One of the advantages in HA being the candidate for biomedical practices, especially as wound dressings, is the superior biocompatibility. And this has much to do with the structure of HA containing plentiful carboxyl and hydroxyl groups, endowing it with a highly hydrophilic property. This property enables HA to retain water for favorable cell growth, as well as absorbing exudate, promoting nutrient exchange, and enhancing cell adhesion [33–35]. Here, the cytotoxicity of each component in hydrogel dressing is determined in naive BMDMs. As shown in Fig. 3A and B, BMDMs show a good cell viability after 48 h of hydrogel treatment. Likewise, no cytotoxicity is found in the allogeneic M2M. In fact, M2M harboring the complete protein profile from the plasma membrane of parent cells can act as a cellular junction, and should promote cell-cell and cell-environment interaction for a better cell adhesion, proliferation, and differentiation [36]. Meanwhile, it concerns us that M2M could potentially interfere with the growth of M1 macrophages derived from BMDMs. Because the almost-forced enhancement in repolarization of M1 macrophages into M2 state driven by M2M could possibly lead to proliferation attenuation due to the balanced proliferative and differentiative course [37]. Therefore, we do further research by treating M1 macrophages, which are matured from BMDMs, with M2M, HAMA, and M2M@HAMA hydrogel for 48 h. In Fig. S7, the M1 macrophages show a good cell viability, and no sign of suppression can be seen in their proliferation.

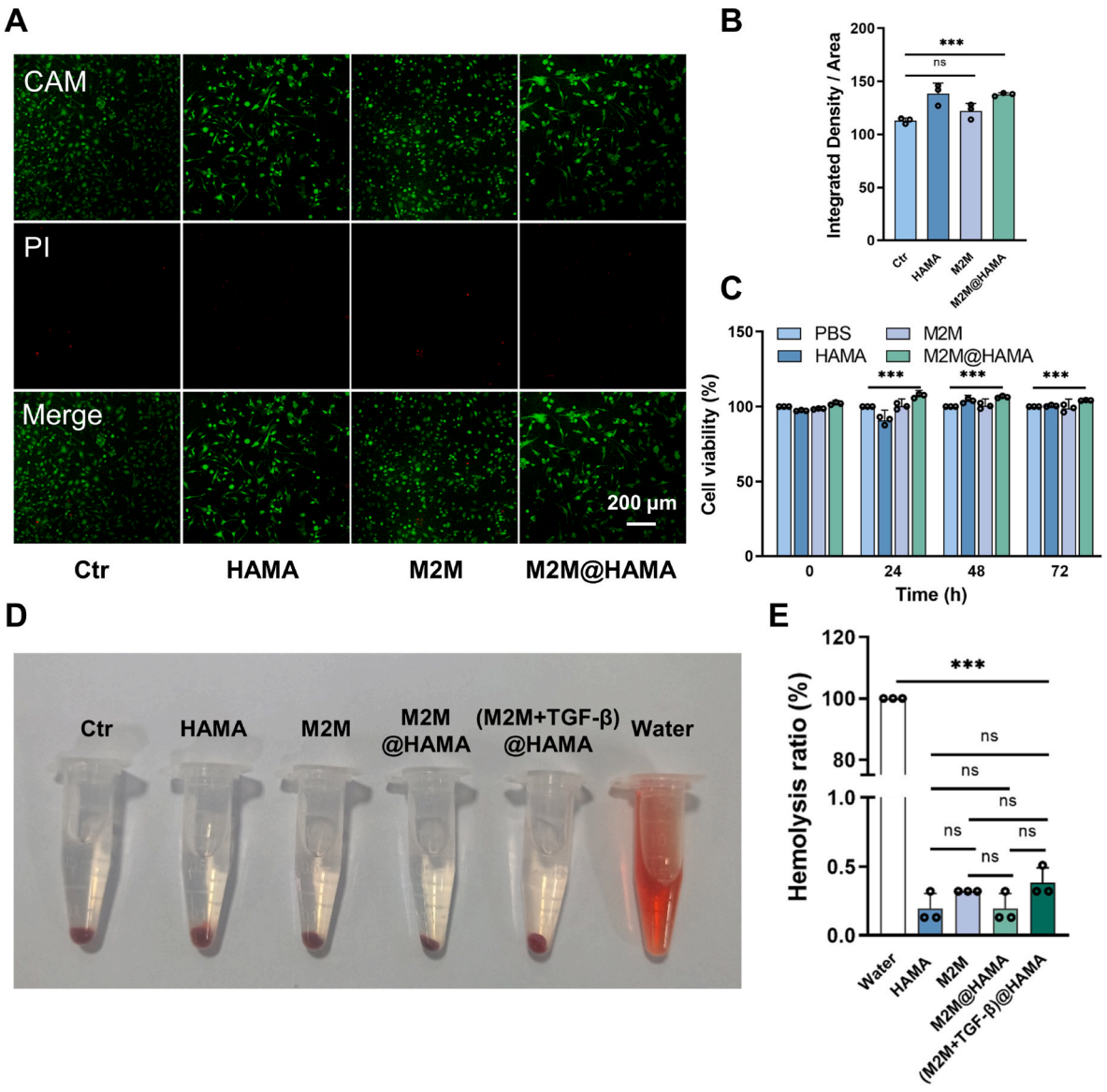

Fig. 3. The HAMA hydrogel and cell membrane show excellent biocompatibility. A) Fluorescent images and B) the corresponding quantitative fluorescence (green) of living/dead cell staining of BMDMs (M0 phenotype) treated for 48 h. Living cells are stained with Calcein-AM in green, and dead cells are stained with PI in red. Scale bar = 200 μm. C) The cell viability of BMDMs (M0 phenotype) determined by CCK8 assay. D) Photographs and E) the corresponding quantitative data in hemolysis test. Data are presented as mean ± SD (n = 3). 'Ctr' represents untreated group. '*' is the intergroup comparison. *, $p < 0.05$; **, $p < 0.01$; ***, $p < 0.001$.

Plus, M2M, HAMA, and M2M@HAMA have demonstrated excellent biocompatibility to the cellular growth of BMDMs in all three subsets (M0 in Fig. 3C, M1 in Fig. S8, and M2 in Fig. S9) via CCK8 assay. They also show remarkable biosafety in the hemolysis test (Fig. 3D and E), even when the solid content of HAMA is adjusted to high levels (Fig. S10). Intriguingly, the BMDMs derived from bone marrow of BALB/c mice are shown to proliferate so slowly even in the Ctr group (Fig. 3C and Fig. S8, S9). In our speculation, unlike mesenchymal cells with rapid proliferating capacity, immune cells (or inflammatory cells) like macrophages are rarely found *in vivo*, and usually exist in a small number, unless the host is confronted with emergencies such as severe wound damage [38,39]. Therefore, primary BMDMs derived from heathy mice are more like maintained in a quiescent state, showing a low growth rate, but can be modulated into different subtypes (such as M1 or M2).

3.4. (M2M + TGF-β) @HAMA hydrogel dressing promotes skin wound healing

Wound healing has long been viewed as an array of physiological events that connection between the preceding and the following is important [40]. So far, HAMA hydrogel has provided spatial-temporal modulation on the physical side, also acting as the main responder answering for protection against infection. And M2M dispersed in hydrogel is responsible for creating an overall epigenetic microenvironment that reverses the pro-inflammatory pathosis. Beyond that, the initiation of fibroblastic proliferation is also crucial for following matrix remodeling and neo-vascularization. So, we use TGF-β as the loading cytokine to aid in cellular proliferation, granulation tissue formation, and angiogenesis. The *in vivo* healing effect of (M2M + TGF-β) @HAMA hydrogel dressing is determined in the inflammatory wound model built in BALB/c mice. Briefly, *E. coli* solution is used to cause bacterial infection in the wound. When an evident inflammation is seen at the wounded site, the wound skin is treated with PBS, M2M, M2M@HAMA, and (M2M + TGF-β)@HAMA, respectively. The hydrogel dressing can be patched on the surface of wound through in-situ gelation by exposing to UV light. After 24 h, the wound dressings are removed. Fig. 4A shows the treatment schedule for animal study. In the representative photographs (Fig. 4B), simulated images (Fig. 4C), and statistical wound closure results (Fig. 4D) of retrieved wound tissues, (M2M + TGF-β)@HAMA shows the strongest effect on promoting wound healing. Inflammation in Ctr is significantly more severe than that in the other groups within 48 h, and M2M manages to control inflammation in the first 2 days. In addition, the intergroup healing rate shows no significance within the first 48 h. Until the 4^{th} day, M2M − and (M2M + TGF-β)@HAMA-treated wounds begin to show an obviously accelerated healing. This suggests to a speeding transformation of innate macrophages into M2 phenotype, thereby expediting inflammation process. From now on, TGF-β begins to intervene fibroblastic proliferation and migration. Thus, the wound healing rate of (M2M + TGF-β)@HAMA-treated mice eventually transcends the other groups. In H&E staining images shown in Fig. 4E, the wound area of (M2M + TGF-β)@HAMA-treated group is smaller than that of other groups at 12 d, which is consistent with the above results in Fig. 4B–D. In normal skin structure, collagen fibers are usually divided into type I and type III, and type I is considered the main component of skin tissue matrix [41]. The Masson staining results (Fig. 4F and Fig. S11, S12) show a growing collagen deposition in the (M2M + TGF-β)@HAMA-treated wounds from 6 d to 12 d. And collagen deposition is significantly increased comparing to other groups in the late stage of healing (12 d), which further indicates to its positive effect on ECM remodeling. Generally, these results suggest that (M2M + TGF-β) @HAMA hydrogel dressing can accelerate inflammation process by releasing massive cell membranes derived from M2 macrophages, and regulate the proliferation and migration of innate fibroblasts for a synergistic improvement of tissue regeneration and wound repair.

3.5. (M2M + TGF-β)@HAMA hydrogel dressing regulates the polarization of endogenous macrophages

The *in vivo* chronic inflammatory conditions are known to generate both intrinsic and extrinsic signals that trigger the context-dependent M1-M2 transition, and the polarization of these macrophages is greatly shaped by specific signaling events that are unique to their niches [42,43]. To amend the excessive inflammation defined by dysregulated wound, anti-infection is by prior arrangement, and then activation of macrophages with anti-inflammatory features. In animal study, the treated wound tissues are retrieved for flow cytometry assay. And $CD45^+$ $CD11b^+$ cell populations are sorted and identified as macrophages (Figs. S13 and S14). For acute wound healing, during the first day of injury when inflammation is most severe, the anti-inflammatory M2 macrophages are normally with a small population in Ctr group (~13.70 % in Fig. 5A). Whereas the M2M − , M2M@HAMA-, and (M2M + TGF-β)@HAMA-treated wounds have a significant increase in M2 macrophage population (Fig. 5A and C). It is worth noting that HA also causes the increase of M2 macrophages, suggesting the known mechanism that HA can affect the activation state of macrophages [44]. Until the 2nd day of injury, the population of M2 macrophages has begun to increase in Ctr (~52.45 % in Fig. 5A), indicating to a hysteretic inflammation process. Meanwhile, the M2 macrophages are continuing to proliferate in the other groups (Fig. 5A and D). Furthermore, the fluorescent staining images of ARG1 and iNOS from wound tissues testify the M1 macrophage attenuation and M2 macrophage supplementation in the treated mice, as well as the stubbornly high population of M1 macrophage in Ctr (Fig. 5B, E, 5F). These data confirm the *in vivo* remodeling effect of M2M on the polarization of endogenous macrophages. In fact, local regulation has advantages in creating the environmental niches that can reverse deep-rooted disorders in chronic wounds. Here, cell membrane is proven a powerful toolkit that inflicts robust normalizing effect on the innate macrophages with versatile phenotypes. Moreover, cell membrane inherits excellent biofunctions from parent cells, while averting potential risks that might be caused by direct delivery of living cells.

3.6. (M2M + TGF-β)@HAMA hydrogel dressing enhances fibroblastic activation and neo-vascularization

Normally, the accelerated inflammatory events should have expedited the overall pathophysiological healing progress [45,46]. From previous study, the transition from predominantly pro-inflammatory macrophages (M1-like phenotype), which present early post-injury, to anti-inflammatory macrophages (M2-like phenotype), which refer to late stage of inflammation, are evidently seen in the wound tissues treated with our hydrogel dressing. In addition to inflammation, understanding and harnessing fibroblastic activation and neo-vascularization may help to advance new approaches for optimal wound healing. In the immunofluorescent images of α-SMA and CD31 (Fig. 6A), the increase of α-SMA in the treated groups indicates to the transition of fibroblasts into myofibroblasts, which hallmarks the fibroblastic activation that leads to production of matrix components [47]. Moreover, the treated groups also show an obvious increase of CD31, which is known as a sensitive and specific marker of vascular differentiation [48]. The immunohistochemical results in Fig. 6B also support such conclusions. It is worth mentioning that (M2M + TGF-β) @HAMA hydrogel dressing demonstrates a strong promoting effect on fibroblastic activation since day 6 (Fig. 6A and D). And a significant neo-vascularization can be seen in the treated groups by day 12 (Fig. 6A–C, 6F, 6G). At the same time, blood vessel density and number are higher in these treated groups (Fig. 6E). In brief, (M2M + TGF-β) @HAMA hydrogel dressing displays an optimal wound healing outcome comparing to other groups, owing to the sequential improvements in healing progress. First, a protective screen is provided by hydrogel dressing against repeating bacterial infection. And then a rapid clearing

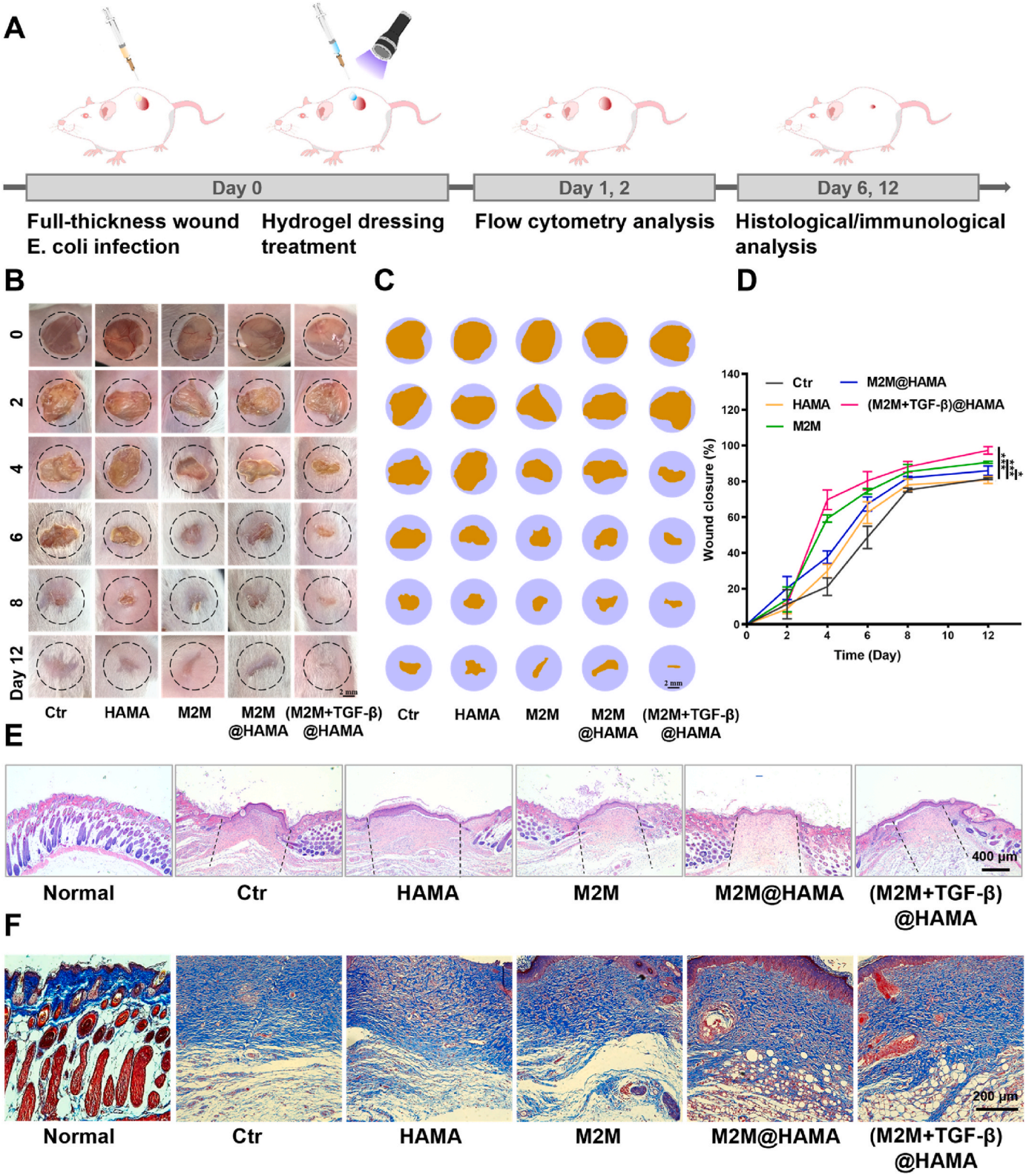

Fig. 4. (M2M + TGF-β)@HAMA hydrogel dressing promotes *in vivo* skin wound healing. A) Schematic diagram of animal study. B) The representative photographs, C) simulated images, and D) quantitative wound closure rate of wound tissues. E) The H&E staining images of wound tissues at 12 d. Scale bar = 400 μm. F) The Masson staining images of wound tissues at 12 d. Scale bar = 200 μm. Data are presented as mean ± SD (n = 3). 'Ctr' represents untreated group. '*' is the intergroup comparison. *, $p < 0.05$; **, $p < 0.01$; ***, $p < 0.001$.

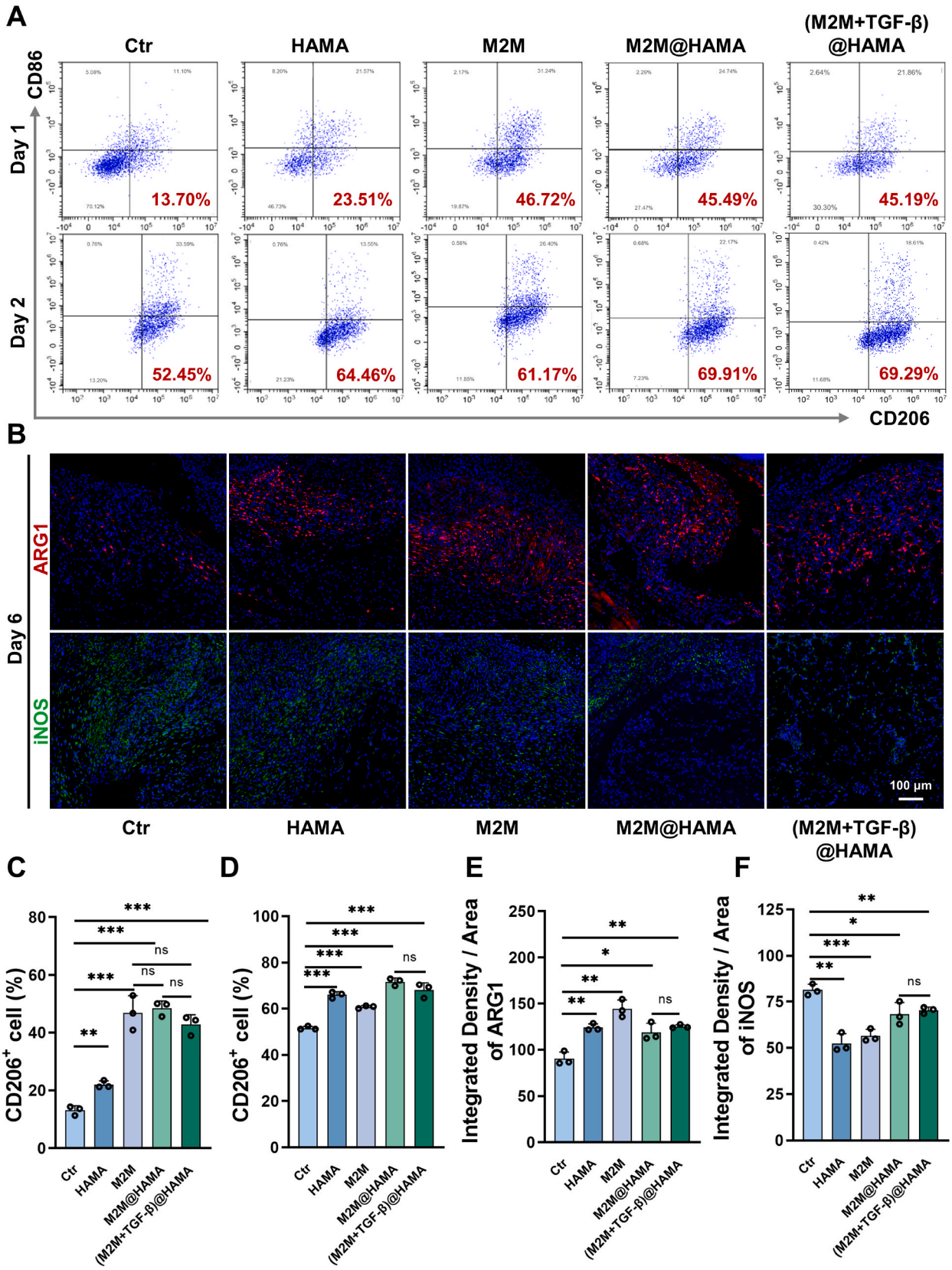

Fig. 5. (M2M + TGF-β)@HAMA hydrogel dressing drives M2-polarization of endogenous macrophages. A) The changes in M1 ($CD86^+$) and M2 ($CD206^+$) macrophage population determined by flow cytometry assay at 1 d and 2 d. B) The immunofluorescent images of ARG1 and iNOS at 6 d. ARG1 is stained in red, iNOS is stained in green, and cell nuclei is stained with DAPI in blue. C) The corresponding quantitative data of M2 macrophages ($CD206^+$) calculated from A) at 1 d. D) The corresponding quantitative data of M2 macrophages ($CD206^+$) calculated from A) at 2 d. E) The corresponding quantitative fluorescence of ARG1 calculated from B). F) The corresponding quantitative fluorescence of iNOS calculated from B). Data are presented as mean ± SD (n = 3). 'Ctr' represents untreated group. '*' is the intergroup comparison. *, $p < 0.05$; **, $p < 0.01$; ***, $p < 0.001$.

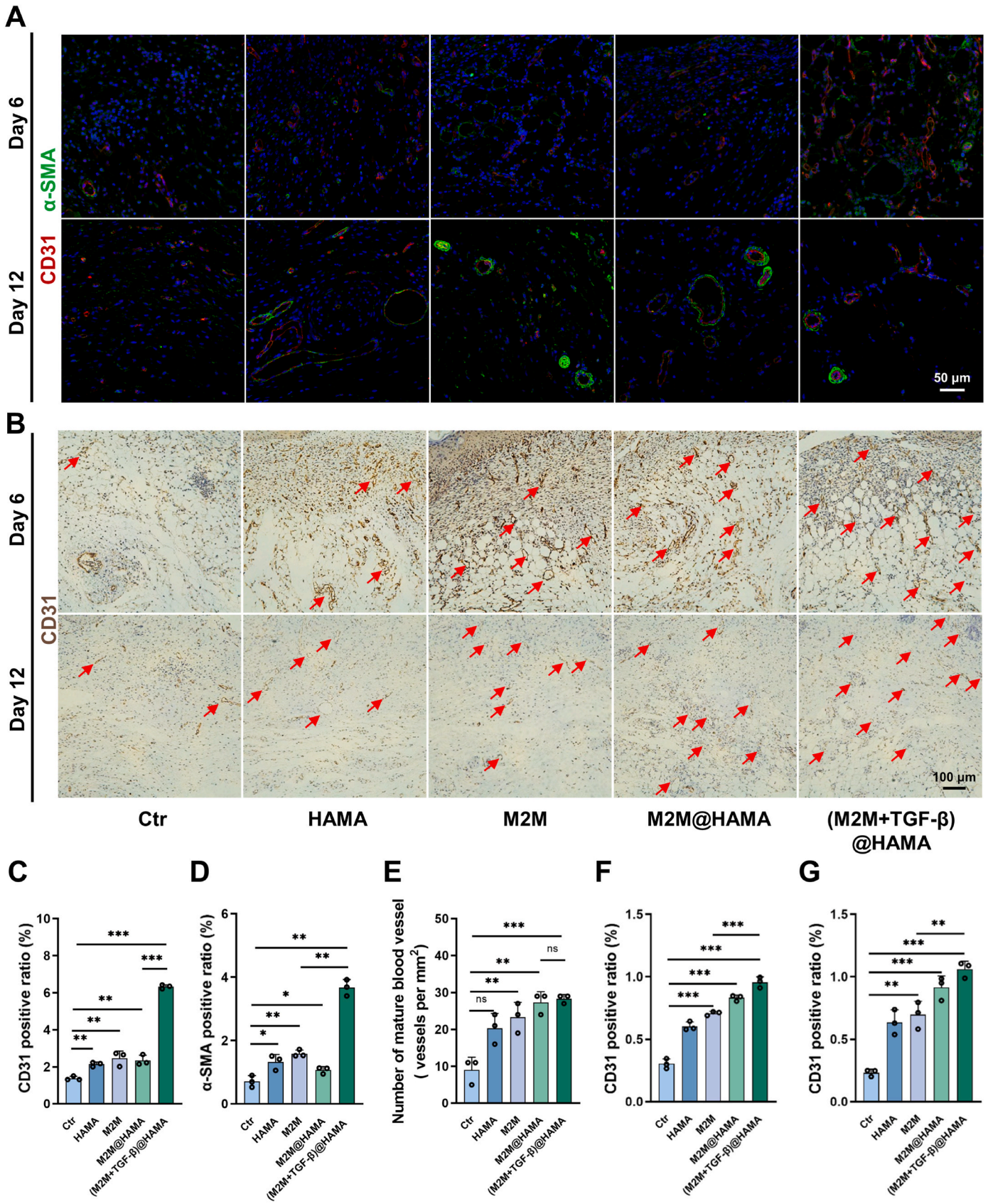

Fig. 6. (M2M + TGF-β)@HAMA hydrogel dressing enhances fibroblastic activation and angiogenesis. A) The immunofluorescent images of α-SMA and CD31 at 6 d and 12 d. α-SMA is stained in green, CD31 is stained in red, and cell nuclei is stained with DAPI in blue. Scale bar = 50 μm. B) The immunohistochemical images of CD31 at 6 d and 12 d. Scale bar = 100 μm. C), D) The corresponding quantitative fluorescence of CD31 and α-SMA calculated from A) at 6 d. E) The corresponding quantitative number of mature blood vessels calculated from A) at 12 d. F), G) The corresponding quantitative CD31 positive area calculated from B) at 6 d and 12 d. Data are presented as mean ± SD (n = 3). 'Ctr' represents untreated group. '*' is the intergroup comparison. *, $p < 0.05$; **, $p < 0.01$; ***, $p < 0.001$.

of bacteria and cell debris is completed by the degradation of HA-based polymer with low molecular weight. Next, cell membranes derived from M2 macrophages (M2M) create remodeling niches for endogenous macrophages that expedite inflammatory events. And eventually, the superior fibroblastic activation and neo-vascularization regulated by TGF-β contribute to an advanced matrix reconstruction and wound closure.

4. Conclusion

In summary, we have successfully developed a biocompatible (M2M + TGF-β)@HAMA hydrogel dressing to improve the outcomes of dysregulated chronic wound healing. Hyaluronic acid-based hydrogel acts as the scaffold material to provide physical coverage over the open wound, preventing it from repeating bacterial infection. The short-chain HA can also clear local bacteria and damaged cell debris in the early post-injury stage. Importantly, cell membranes derived from M2 macrophages can be aggregated in the HA hydrogel to create M2-like niches that help to drive macrophages in versatile subtypes toward M2 phenotype, the continuous inflammation in refractory wound is then accelerated. Subsequently, TGF-β loaded in the hydrogel intervenes with the following stage of fibroblastic activation, initiating matrix remodeling, angiogenesis, and granulation tissue formation. Thus, the overall healing progress is expedited, averting chronic healing or even non-healing from happening. The (M2M + TGF-β)@HAMA hydrogel dressing is proven an effective product to elicit a positive response from innate macrophages by creating an epigenetic microenvironment. It possesses a promising future for clinical use and might have a broad application in tissue engineering and biomedical research.

CRediT authorship contribution statement

Yijuan Ding: Writing – original draft, Methodology, Investigation, Formal analysis, Data curation. **Qi Jia:** Writing – review & editing, Methodology, Investigation, Formal analysis, Data curation. **Ziwen Su:** Validation, Investigation, Formal analysis. **Heying Chen:** Investigation. **Jialing Ye:** Investigation, Data curation. **Dafeng Xie:** Visualization. **Yubo Wu:** Supervision. **Haiyan He:** Resources. **Yanlin Peng:** Resources. **Yilu Ni:** Writing – review & editing, Validation, Supervision, Project administration, Funding acquisition, Conceptualization.

Declaration of competing interest

The authors declare that they have no known competing financial interests or personal relationships that could have appeared to influence the work reported in this paper.

Data availability

Data will be made available on request.

Acknowledgements

This work is financially supported by National Natural Science Foundation of China (No. 82203017), Natural Science Foundation of Chongqing Municipality (No. CSTB2023NSCQ-MSX0269), and Science & Technology Research Project of Chongqing Municipal Education Commission (KJQN202200408). All animal experiments were conducted under protocols approved by the Institutional Animal Care and Use Committee of Chongqing Medical University's School of Medicine.

The data to support the conclusions are present in the main text and supplementary materials. Additional data related to this work may be requested from the authors.

Appendix A. Supplementary data

Supplementary data to this article can be found online at https://doi.org/10.1016/j.mtbio.2024.101243.

References

[1] T.N. Demidova-Rice, M.R. Hamblin, I.M. Herman, Acute and impaired wound healing, Adv. Skin Wound Care 25 (2012) 304–314, https://doi.org/10.1097/01.ASW.0000416006.55218.d0.
[2] R.F. Diegelmann, Wound healing: an overview of acute, fibrotic and delayed healing, Front. Biosci. 9 (2004) 283–289, https://doi.org/10.2741/1184.
[3] A. Stojadinovic, J.W. Carlson, G.S. Schultz, et al., Topical advances in wound care, Gynecol. Oncol. 111 (2008) S70–S80, https://doi.org/10.1016/j.ygyno.2008.07.042.
[4] S.A. Eming, T. Krieg, J.M. Davidson, Inflammation in wound repair: molecular and cellular mechanisms, J. Invest. Dermatol. 127 (2007) 514–525, https://doi.org/10.1038/sj.jid.5700701.
[5] W.M. Van der Veer, M.C.T. Bloemen, M.M.W. Ulrich, et al., Potential cellular and molecular causes of hypertrophic scar formation, Burns 35 (2009) 15–29, https://doi.org/10.1016/j.burns.2008.06.020.
[6] P. Krzyszczyk, R. Schloss, A. Palmer, et al., The role of macrophages in acute and chronic wound healing and interventions to promote pro-wound healing phenotypes, Front. Physiol. 9 (2018) 419, https://doi.org/10.3389/fphys.2018.00419.
[7] A. Hassanshahi, M. Moradzad, S. Ghalamkari, et al., Macrophage-mediated inflammation in skin wound healing, Cells 11 (2022) 2953, https://doi.org/10.3390/cells11192953.
[8] K.M. Vannella, T.A. Wynn, Mechanisms of organ injury and repair by macrophages, Annu. Rev. Physiol. 79 (2017) 593–617, https://doi.org/10.1146/annurev-physiol-022516-034356.
[9] G. Kwak, J. Cheng, H. Kim, et al., Sustained exosome-guided macrophage polarization using hydrolytically degradable PEG hydrogels for cutaneous wound healing: identification of key proteins and MiRNAs, and sustained release formulation, Small 18 (2022) e2200060, https://doi.org/10.1002/smll.202200060.
[10] Y. Qian, Y. Zheng, J. Jin, et al., Immunoregulation in diabetic wound repair with a photoenhanced glycyrrhizic acid hydrogel scaffold, Adv. Mater. 34 (2022) e2200521, https://doi.org/10.1002/adma.202200521.
[11] Y. Wu, Y. Wang, C. Zheng, et al., A versatile glycopeptide hydrogel promotes chronic refractory wound healing through bacterial elimination, sustained oxygenation, immunoregulation, and neovascularization, Adv. Funct. Mater. 33 (2023) 2305992, https://doi.org/10.1002/adfm.202305992.
[12] F. Motsoene, H. Abrahamse, S.S. Dhilip Kumar, Multifunctional lipid-based nanoparticles for wound healing and antibacterial applications: a review, Adv. Colloid Interface Sci. 321 (2023) 103002, https://doi.org/10.1016/j.cis.2023.103002.
[13] J. Lin, Z. Lin, L. Liu, et al., Enhancing glioma-specific drug delivery through self-assembly of macrophage membrane and targeted polymer assisted by low-frequency ultrasound irradiation, Mater. Today Bio. 26 (2024) 101067, https://doi.org/10.1016/j.mtbio.2024.101067.
[14] Y. Han, H. Pan, W. Li, et al., T cell membrane mimicking nanoparticles with bioorthogonal targeting and immune recognition for enhanced photothermal therapy, Adv. Sci. 6 (2019) 1900251, https://doi.org/10.1002/advs.201900251.
[15] J.M. Pitt, F. André, S. Amigorena, et al., Dendritic cell–derived exosomes for cancer therapy, J. Clin. Invest. 126 (2016) 1224–1232, https://doi.org/10.1172/jci81137.
[16] J. Wang, J. Yang, K. Liu, et al., Tumor targeted cancer membrane-camouflaged ultra-small fe nanoparticles for enhanced collaborative apoptosis and ferroptosis in glioma, Mater. Today Bio. 22 (2023) 100780, https://doi.org/10.1016/j.mtbio.2023.100780.
[17] J. Dai, Z. Chen, S. Wang, et al., Erythrocyte membrane-camouflaged nanoparticles as effective and biocompatible platform: either autologous or allogeneic erythrocyte-derived, Mater, Today Bio. 15 (2022) 100279, https://doi.org/10.1016/j.mtbio.2022.100279.
[18] W. Zhang, X. Huang, Stem cell membrane-camouflaged targeted delivery system in tumor, Mater, Today Bio. 16 (2022) 100377, https://doi.org/10.1016/j.mtbio.2022.100377.
[19] P.J. Murray, Macrophage polarization, Annu. Rev. Physiol. 79 (2017) 541–566, https://doi.org/10.1146/annurev-physiol-022516-034339.
[20] D. Wang, M. Xue, J. Chen, et al., Macrophage-derived implantable vaccine prevents postsurgical tumor recurrence, Biomaterials 278 (2021) 121161, https://doi.org/10.1016/j.biomaterials.2021.121161.
[21] C. Yunna, H. Mengru, W. Lei, et al., Macrophage M1/M2 polarization, Eur. J. Pharmacol. 877 (2020) 173090, https://doi.org/10.1016/j.ejphar.2020.173090.
[22] D. Wang, H. Chen, L. Lei, et al., Biofabricated macrophage and fibroblast membranes synergistically promote skin wound healing, Bioeng. Transl. Med. 7 (2022) e10344, https://doi.org/10.1002/btm2.10344.
[23] A.G. Tavianatou, I. Caon, M. Franchi, et al., Hyaluronan: molecular size-dependent signaling and biological functions in inflammation and cancer, FEBS J. 286 (2019) 2883–2908, https://doi.org/10.1111/febs.14777.
[24] H. Dong, C. Feng, J. Zhu, et al., Ultrasmall gold nanoparticles/carboxymethyl chitosan composite hydrogel: tough, restorable, biocompatible antimicrobial

dressing for wound healing, Appl. Mater. Today 38 (2024) 102206, https://doi.org/10.1016/j.apmt.2024.102206.
[25] H. Knopf-Marques, M. Pravda, L. Wolfova, et al., Hyaluronic acid and its derivatives in coating and delivery systems: applications in tissue engineering, regenerative medicine and immunomodulation, Adv. Healthc. Mater. 5 (2016) 2841–2855, https://doi.org/10.1002/adhm.201600316.
[26] L. He, J. Yang, J. Lu, et al., Preparation and characterization of a novel hyaluronic acid–icariin conjugate hydrogel, Mater. Lett. 136 (2014) 41–44, https://doi.org/10.1016/j.matlet.2014.08.006.
[27] X. Zhang, D. Wei, Y. Xu, et al., Hyaluronic acid in ocular drug delivery, Carbohydr. Polym. 264 (2021) 118006, https://doi.org/10.1016/j.carbpol.2021.118006.
[28] G.F. Pierce, Inflammation in nonhealing diabetic wounds: the space-time continuum does matter, Am. J. Pathol. 159 (2001) 399–403, https://doi.org/10.1016/s0002-9440(10)61709-9.
[29] H. Al Sadoun, Macrophage phenotypes in normal and diabetic wound healing and therapeutic interventions, Cells 11 (2022) 2430, https://doi.org/10.3390/cells11152430.
[30] G.V. Ganesh, K.M. Ramkumar, Macrophage mediation in normal and diabetic wound healing responses, Inflamm. Res. 69 (2020) 347–363, https://doi.org/10.1007/s00011-020-01328-y.
[31] J. Van den Bossche, J. Baardman, A. Otto Natasja, et al., Mitochondrial dysfunction prevents repolarization of inflammatory macrophages, Cell Rep. 17 (2016) 684–696, https://doi.org/10.1016/j.celrep.2016.09.008.
[32] A. Fallacara, E. Baldini, S. Manfredini, et al., Hyaluronic acid in the third millennium, Polymers 10 (2018) 701, https://doi.org/10.3390/polym10070701.
[33] M. Mahedia, N. Shah, B. Amirlak, Clinical evaluation of hyaluronic acid sponge with zinc versus placebo for scar reduction after breast surgery, Plast. Reconstr. Surg. Glob. Open. 4 (2016) e791, https://doi.org/10.1097/gox.0000000000000747.
[34] A. Mohandas, B.S. Anisha, K.P. Chennazhi, et al., Chitosan–hyaluronic acid/VEGF loaded fibrin nanoparticles composite sponges for enhancing angiogenesis in wounds, Colloids Surf. B Biointerfaces 127 (2015) 105–113, https://doi.org/10.1016/j.colsurfb.2015.01.024.
[35] Z. Zhu, Y.-M. Wang, J. Yang, et al., Hyaluronic acid: a versatile biomaterial in tissue engineering, Plast. Aesthet. Res. 4 (2017) 219–227, https://doi.org/10.20517/2347-9264.2017.71.
[36] P.R. Taylor, L. Martinez-Pomares, M. Stacey, et al., Macrophage receptors and immune recognition, Annu. Rev. Immunol. 23 (2005) 901–944, https://doi.org/10.1146/annurev.immunol.23.021704.115816.
[37] R. Gentek, K. Molawi, M.H. Sieweke, Tissue macrophage identity and self-renewal, Immunol. Rev. 262 (2014) 56–73, https://doi.org/10.1111/imr.12224.
[38] A.A.J. Hamers, A.B. Pillai, A sweet alternative: maintaining M2 macrophage polarization, Sci. Immunol. 3 (2018) eaav7759, https://doi.org/10.1126/sciimmunol.aav7759.
[39] C.E. Witherel, D. Abebayehu, T.H. Barker, et al., Macrophage and fibroblast interactions in biomaterial-mediated fibrosis, Adv. Healthc. Mater. 8 (2019) e1801451, https://doi.org/10.1002/adhm.201801451.
[40] Y.H. Almadani, J. Vorstenbosch, P.G. Davison, et al., Wound healing: a comprehensive review, Semin. Plast. Surg. 35 (2021) 141–144, https://doi.org/10.1055/s-0041-1731791.
[41] S.S. Mathew-Steiner, S. Roy, C.K. Sen, Collagen in wound healing, Bioengineering (Basel) 8 (2021) 63, https://doi.org/10.3390/bioengineering8050063.
[42] W. Xu, X. Zhao, M.R. Daha, et al., Reversible differentiation of pro- and anti-inflammatory macrophages, Mol. Immunol. 53 (2013) 179–186, https://doi.org/10.1016/j.molimm.2012.07.005.
[43] L. Zhang, C.C. Wang, Inflammatory response of macrophages in infection, Hepatob. Pancreat Dis. Int. 13 (2014) 138–152, https://doi.org/10.1016/s1499-3872(14)60024-2.
[44] J.E. Rayahin, J.S. Buhrman, Y. Zhang, et al., High and low molecular weight hyaluronic acid differentially influence macrophage activation, ACS Biomater. Sci. Eng. 1 (2015) 481–493, https://doi.org/10.1021/acsbiomaterials.5b00181.
[45] Y. Li, J. Wang, D. Qian, et al., Electrospun fibrous sponge via short fiber for mimicking 3D ECM, J. Nanobiotechnol. 19 (2021) 131, https://doi.org/10.1186/s12951-021-00878-5.
[46] B. Mi, L. Chen, Y. Xiong, et al., Saliva exosomes-derived UBE2O mRNA promotes angiogenesis in cutaneous wounds by targeting SMAD6, J. Nanobiotechnol. 18 (2020) 68, https://doi.org/10.1186/s12951-020-00624-3.
[47] M. D'Urso, N.A. Kurniawan, Mechanical and physical regulation of fibroblast–myofibroblast transition: from cellular mechanoresponse to tissue pathology, Front. Bioeng. Biotechnol. 8 (2020) 609653, https://doi.org/10.3389/fbioe.2020.609653.
[48] Y. Shen, G. Xu, H. Huang, et al., Sequential release of small extracellular vesicles from bilayered thiolated alginate/polyethylene glycol diacrylate hydrogels for scarless wound healing, ACS Nano 15 (2021) 6352–6368, https://doi.org/10.1021/acsnano.0c07714.